BULLETIN DE L'ASSOCIATION MINERALOGIQUE DU CANADA
THE CANADIAN MINERALOGIST
JOURNAL OF THE MINERALOGICAL ASSOCIATION OF CANADA

Volume 34 August 1996 Part 4

The Canadian Mineralogist
Vol. 34, pp. 697-716 (1996)

SILVER IN SULFIDE CHIMNEYS AND MOUNDS FROM 13°N AND 21°N, EAST PACIFIC RISE

ROGER MOSS* AND STEVEN D. SCOTT

Marine Geology Research Laboratory, Department of Geology, University of Toronto,
22 Russell Street, Toronto, Ontario M5S 3B1

ABSTRACT

A geochemical and mineralogical study of hydrothermal deposits from 13°N and 21°N, East Pacific Rise was conducted in order to identify controls on the distribution of silver. The 349°C hydrothermal fluid from the Southwest vent field (21°N) is enriched in silver by approximately three orders of magnitude compared to seawater. This silver is shown to be transported as the dichlorosilver(I) complex, and to be undersaturated with respect to Ag_2S. The absence of a separate silver phase such as acanthite in East Pacific Rise chimneys suggests that silver remains undersaturated with respect to Ag_2S during cooling and mixing of the hydrothermal fluid with seawater. However, silver is present to some degree in sulfides occurring throughout the paragenesis of chimney growth, and is therefore controlled by its distribution in precipitating sulfides. Bulk silver content of subsamples from a zoned black smoker from the Southwest vent field near 21°N is accounted for by silver contained in chalcopyrite, pyrite, marcasite and zinc sulfide. Galena has the highest silver concentrations (up to 0.95 wt%), but is present in trace amounts and so does not make a significant contribution to the bulk silver content of the chimney. Bulk chemical analyses of 33 chimney samples gave silver concentrations of up to 206 ppm. Silver shows significant positive correlations with Pb, S, Sb, Cd, Mn and Au in chimneys from both areas. The silver content is also positively correlated with the morphological maturity of structures in which it is contained, being highest in basal mounds and lowest in immature anhydrite-rich chimneys. Thus, silver is continuously enriched in seafloor deposits during the lifetime of the hydrothermal system.

Keywords: silver, sulfides, East Pacific Rise, hydrothermal, seafloor, vents, chimneys, mounds.

SOMMAIRE

Nous avons effectué une étude géochimique et minéralogique des dépôts hydrothermaux le long de la crête Est-Pacifique, aux latitudes 13°N et 21°N, afin d'identifier les facteurs qui régissent la distribution de l'argent. La phase fluide hydrothermale à 349°C du champ d'activité hydrothermale dit Southwest (21°N) montre un enrichissement en Ag par un facteur de trois ordres de grandeur, comparé à l'eau de mer. L'argent y est transporté sous forme de complexe dichloroargenté(I). La phase fluide serait sous-saturée par rapport à Ag_2S. L'absence de phases minérales argentifères distinctes, telle que l'acanthite, dans les cheminées de la crête Est-Pacifique, fait penser que l'argent est demeuré sous-saturé par rapport à Ag_2S lors du refroidissement et du mélange de la phase fluide hydrothermale avec l'eau de mer. Toutefois, l'argent est réparti parmi les sulfures qui sont formés durant la croissance des cheminées, et sa distribution est régie par ces minéraux. Les teneurs globales en Ag des

---

* To whom correspondence should be addressed.

sous-échantillons prélevés d'un évent de type "fumeur noir" dans le champ Southwest, près de 21°N, sont bien expliquées par la teneur en Ag de chalcopyrite, pyrite, marcasite et sulfure de zinc. C'est la galène qui montre les teneurs les plus élevées (jusqu'à 0.95%, en poids), mais elle est présente en quantités infimes, et donc sans importance dans le bilan de l'argent d'une cheminée. Les analyses chimiques globales de 33 échantillons de cheminées montrent des concentrations en Ag allant jusqu'à 206 ppm. La teneur en argent montre des corrélations positives avec les concentrations de Pb, S, Sb, Cd, Mn et Au dans les cheminées des deux endroits. Elle montre aussi une corrélation positive avec la maturité morphologique des structures, étant enrichie dans les amoncellements à la base des structures et beaucoup plus dispersée dans les parties des cheminées à forte teneur en anhydrite. Il paraît donc évident que l'argent est continuellement enrichi dans les dépôts des fonds marins au cours de l'évolution d'un système hydrothermal.

(Traduit par la Rédaction)

Mots-clés: argent, sulfures, crête Est-Pacifique, hydrothermal, fonds marins, évents, cheminées, amoncellements.

INTRODUCTION

Silver is found in volcanogenic massive sulfide (VMS) deposits of all ages and is an important by-product of Cu–Pb–Zn mining. The distribution of silver in ancient VMS deposits has been relatively well studied, generally from an applied mineralogy point of view, in an effort to increase silver recovery during beneficiation (*e.g.*, Harris *et al.* 1984, Cabri *et al.* 1984, Knights & Patterson 1988, Chryssoulis & Surges 1988). In contrast, the silver content of modern VMS deposits has received only cursory attention (Hannington & Scott 1988, Zierenberg & Schiffman 1990), despite the otherwise significant contribution that studies of seafloor deposits have made to our knowledge of the genesis of VMS deposits (see review by Rona & Scott 1993).

An investigation of the distribution of silver in hydrothermal deposits of the East Pacific Rise was undertaken in an effort to understand the mechanisms of silver transport and deposition in a modern hydrothermal system. The East Pacific Rise deposits were chosen because of the availability of data on the chemistry of the associated vent fluids (Michard *et al.* 1984, Von Damm *et al.* 1985a, Bowers *et al.* 1988) which, in the case of 21°N, includes data on the silver content of the fluid. Previous geochemical studies at 21°N (Hekinian *et al.* 1980, Bischoff *et al.* 1983, Oudin 1987, Ortega-Osorio & Paez-Osuna 1989) and at 13°N (Hekinian & Fouquet 1985, Fouquet *et al.* 1988) had shown silver to be present to varying degrees (up to 450 ppm) in the chimneys and mounds comprising the deposits.

GENERAL GEOLOGY

The East Pacific Rise (Fig. 1a) is a sediment-starved mid-ocean ridge that is spreading at a total rate of 6 cm/year at 21°N (Ballard & Francheteau 1982) and at a full rate of 12 cm/year in the vicinity of 13°N (Hekinian *et al.* 1983, Ballard *et al.* 1984). Sulfide deposits were first discovered on the East Pacific Rise at 21°N during the 1978 CYAMEX expedition (Francheteau *et al.* 1979). Subsequent investigations resulted in the discovery of active hydrothermal vent fields along the axis of the East Pacific Rise between latitude 20°49′N and 20°52′N (Spiess *et al.* 1980) and between 11°N and 13°N (Hekinian *et al.* 1983).

To date, four active vent sites have been located in the vicinity of 21°N (Von Damm 1983): National Geographic Smoker (NGS), Ocean Bottom Seismometer (OBS), Southwest (SW) and Hanging Gardens (HG) . All four vent sites occur along the Rise axis (Fig. 1c), and are spatially associated with eruptive fissures (Ballard *et al.* 1981). A topographic high between 20°45′N and 20°47′N separates the NGS, OBS and SW vent sites to the northeast from the HG vent field to the southwest (Ballard & Francheteau 1982). The maximum exit temperatures of hydrothermal fluids, and the highest ratio of sheet flows to pillow flows, indicative of closest proximity to the magmatic source, are found near the topographic high (Ballard & Francheteau 1982). Exit temperatures of vent fluids generally increase from northeast to southwest in the 21°N area. Still further to the northeast, in the CYAMEX area (Fig. 1c), only extinct vents have been found (Francheteau *et al.* 1979, Hekinian *et al.* 1980).

The geology of the active hydrothermal area in the vicinity of 13°N has been described by Hekinian *et al.* (1983, 1984, 1985), Ballard *et al.* (1984), and Gente *et al.* (1986). Approximately eighty hydrothermal deposits occur along a 20-km section of the ridge axis and are generally confined to the central graben (Fig. 1b). Most active deposits are associated with the freshest, most recent lava flows in the so-called "lava-pond" domain. The older "fissural domain" hosts inactive hydrothermal deposits rich in iron oxide and manganese, and is characterized by variably altered pillowed and massive flows.

SAMPLE PREPARATION AND ANALYSIS

Nine chimney samples from 21°N and nine from 13°N were selected for analysis. Chimney samples from 21°N were obtained from Woods Hole Oceanographic Institute and were collected by the submersible *Alvin* during the cruises in 1979 and 1981.

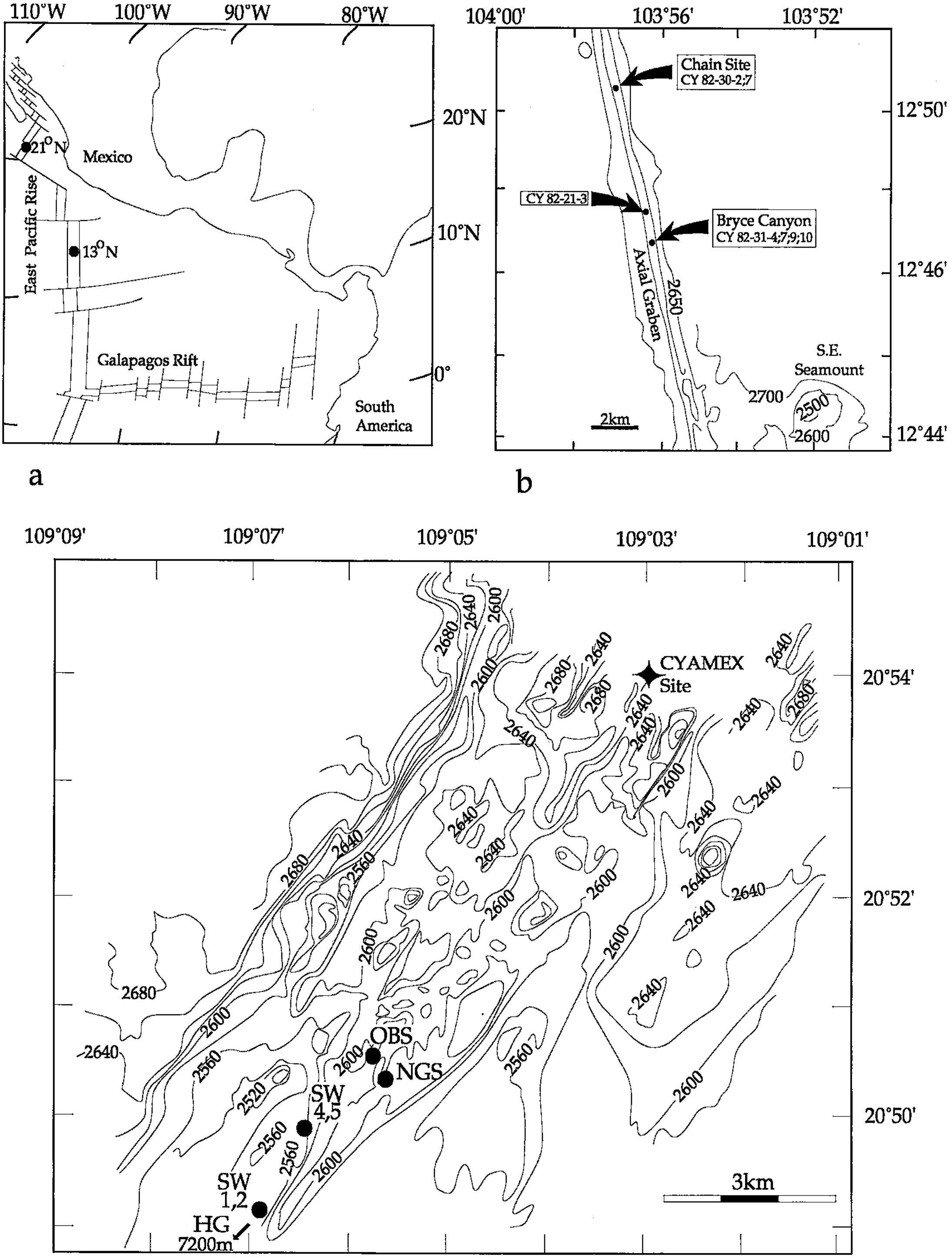

Fig. 1. a) Location of study areas along the East Pacific Rise axis. b) Simplified bathymetric map of the area near 13°N, showing sample localities (modified from Fouquet *et al.* 1988). c) Simplified bathymetric map of the area near 21°N showing location of vent sites: OBS: Ocean Bottom Seismograph, NGS: National Geographic Society, SW: Southwest [modified from Spiess *et al.* (1980), vent coordinates from Von Damm (1983), CYAMEX coordinates from Francheteau *et al.* (1979)].

The 13°N chimney samples collected by the submersible *Cyana* during the 1982 CYATHERM cruise were obtained from IFREMER's Centre de Brest.

Samples were examined by binocular microscope, and those showing strong zonation were selected for detailed mineralogical study. A polished section was prepared for each zone, and the remainder of the subsample was used for chemical analysis. A total of 20 and 13 samples (including subsamples) were analyzed from 21°N and 13°N, respectively (Table 1).

Bulk chemical analysis

Samples were analyzed at the University of Toronto by instrumental neutron-activation analysis (INAA), and commercially at X-ray Assay Laboratories. The INAA technique used was a modification of the method of Hannington & Gorton (1991). Smaller sizes of sample (approximately 50 mg) were used for the 7- and 40- day counts in an attempt to keep counter dead-time to <15%, and samples were contained in flat 1-cm-square plastic "baggies" instead of the vials used

TABLE 1. DESCRIPTIONS OF SAMPLES FROM 13°N AND 21°N EAST PACIFIC RISE

AREA	SAMPLE NO.	DESCRIPTION	BULK MINERALOGY
13°N	CY-82-31-7	Zn-rich chimney	py, ZnS, tr cpy, bn
	CY-82-21-3	Fragment of obtruded Zn-rich edifice	py, ZnS, tr cpy
	CY-82-31-10	Cu-anh-rich chimney (T = 320°C)	
		(a)	cpy-rich, tr bn
		(b)	anh, py, cpy
		(c)	ZnS, py
	CY-82-31-09	Active chimney (T = 330°C)	anh, ZnS, tr py, cpy
	CY-82-31-04	Active chimney (T = 245°C)	
		a	ZnS, tr cpy, bn
		b	ZnS, anh
	CY-82-30-07	Zn-rich chimney	
		a	cpy, py, Zns
		b	py, Zns, Fe oxide
	CY-82-30-02	Active chimney (T=319°C)	anh, cpy, py, tr ZnS
	CY-82-31-5/6	Active Cu anh-rich chimney	cpy, py, anh
21°N	981-R2	section through chimney wall	
		(A) interior chimney wall	cpy-rich
		(B) exterior chimney wall	ZnS, anh, tr cpy
	1149-1-1	(E) chimney piece	ZnS, anh
	1149-2-3	(G) chimney fragment	ZnS' anh, tr cpy
		(F) chimney fragment	anh, ZnS, FeS
	1149-2-18	complete chimney piece	
		(A;A1) interior chimney wall	cpy-rich, tr anh, py
		exterior chimney wall	
		(B;B1)	mc, ZnS, tr anh
		(C;C1)	mc, ZnS, tr cpy, anh
		(D; J)	cpy, py, ZnS
	981-R-1-2	section through chimney	
		(A) exterior chimney wall	anh-rich
		(C) interior chimney wall	ZnS-rich, tr py
	1149-1-1	section through white smoker	
		(A) interior wall	cpy, ZnS
		(B) exterior wall	ZnS, py
	1150-1-1	exterior chimney piece	ZnS-rich
	981-R-20	chimney piece	ZnS, anh
	1148-2#6	chimney piece	anh, ZnS

13°N samples CY 82-30 are from the "Chain Site" and samples prefixed CY 82-31 are from the "Bryce Canyon" Site (Hekinian *et al.* 1984). Descriptions are from Hekinian *et al.* (1984), Fouquet *et al.* (1988) and Fouquet (pers. comm. 1994). 21°N samples are from the South West Vent Field, with the exception of 982-R-20, which is from the National Geographic Society Field. Abreviations: anh = anhydrite, bn = bornite, cpy = chalcopyrite, mc = marcasite, py = pyrite, ZnS = zinc sulfide (undifferentiated sphalerite or wurtzite), tr = trace.

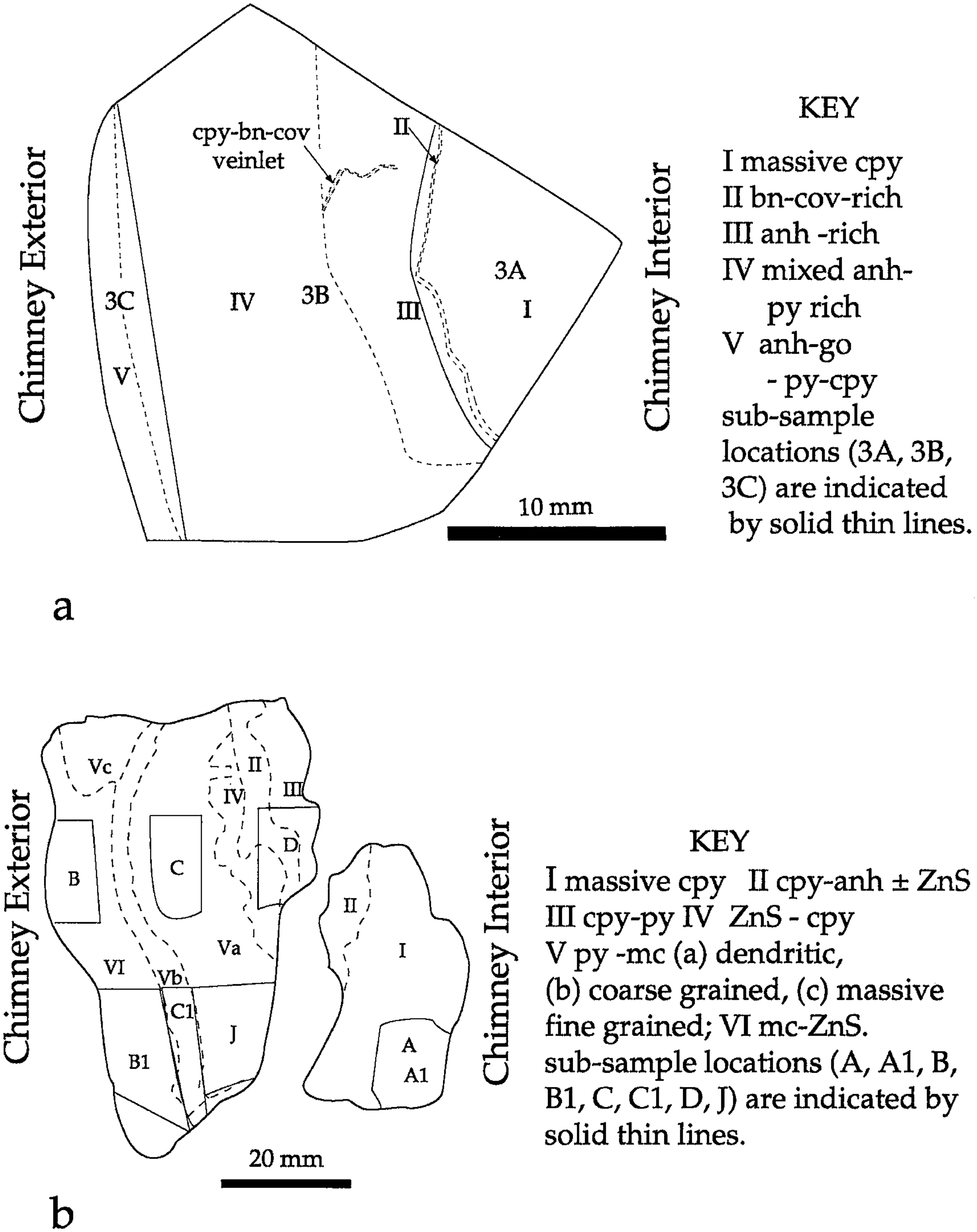

FIG. 2. Schematic cross-section through a) chimney CY82–31–10 from Bryce Canyon, 13°N East Pacific Rise, and b) chimney 1149–2–18 from the Southwest vent Site at 21°N. Symbols: anh anhydrite, bn bornite, cpy chalcopyrite, cov covellite, mc marcasite, py pyrite, ZnS zinc sulfide.

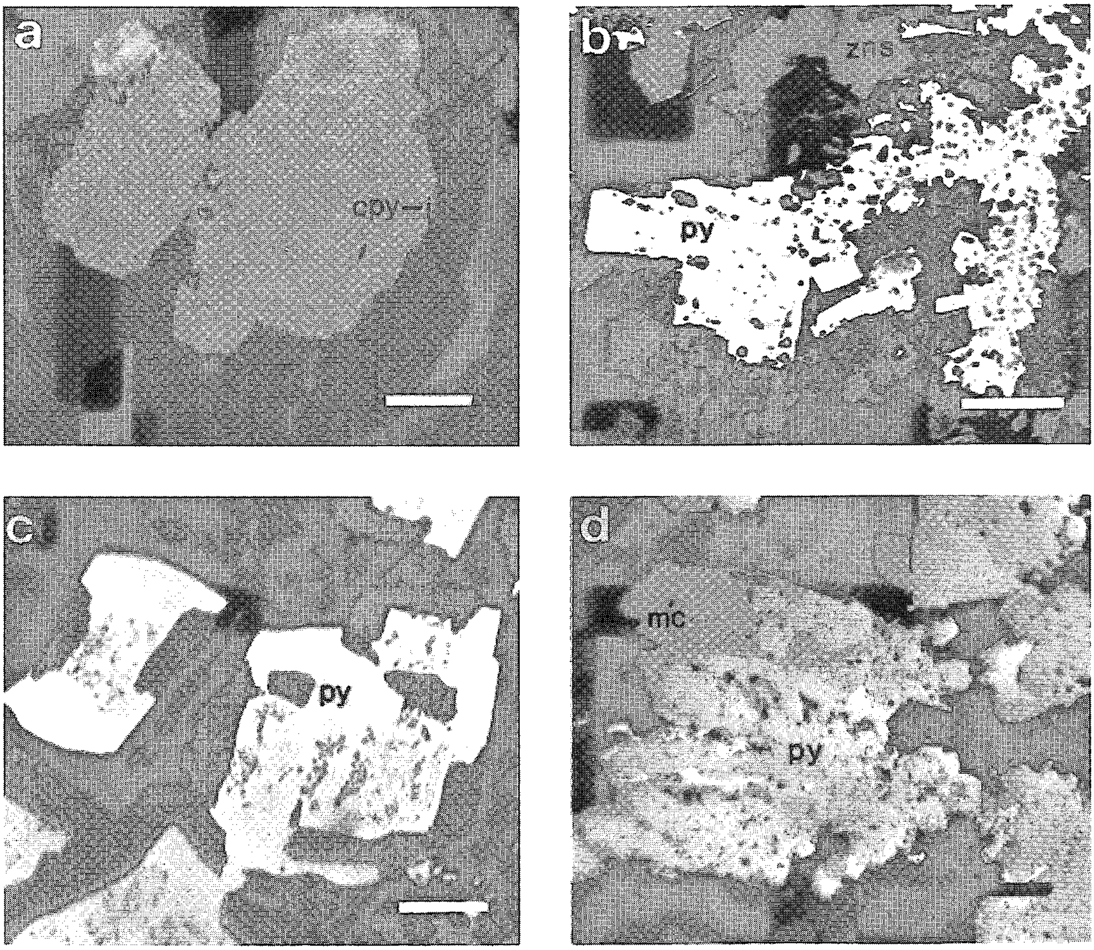

by Hannington & Gorton (1991). Approximately 150 mg of sample were used for short counts (3-minute irradiation and 3-minute counting time) for determination of Mn, Mg, Al and In concentrations, as counter dead-time was not a problem in this case.

Precision of all analyses, checked by analysis of replicates, was found to vary by element. In general, analyses of samples for Cu, S, Ca, As, Sr and Mn give results in agreement to better than 5%, for Au, Al, Co, Mo, Na, Fe and Si, to better than 10%, with the remainder having a precision of less than 10%. The precision of the Ag determinations was 14%. INAA analyses for Ag in a suite of CANMET sulfide standards gave 2.5 to 7% deviation from the recommended value.

Electron-microprobe analysis

Wavelength-dispersion electron-microprobe analyses (EMPA) of minerals in representative sections were carried out using the Cameca SX50 at the University of Toronto. As operating conditions changed for the various minerals analyzed, the minimum detection-limit (MDL) for silver and the precision of the results varied accordingly.

Modal percentages of major minerals in zones of chimney sample 1149–2–18 were determined by image analysis. Back-scattered, secondary electron and X-ray images collected with the Cameca SX50 were analyzed using the *visilog* image-processing routine in combination with the *scatter* and *xyreccon* subroutines (J.C. Rucklidge, unpubl.).

Proton-microprobe analysis

Because minimum limits of detection of less than 100 ppm for silver in major sulfide minerals were unachievable with the electron microprobe, a proton microprobe at the University of Guelph was used to analyze sulfides from chimney sample 1149–2–18.

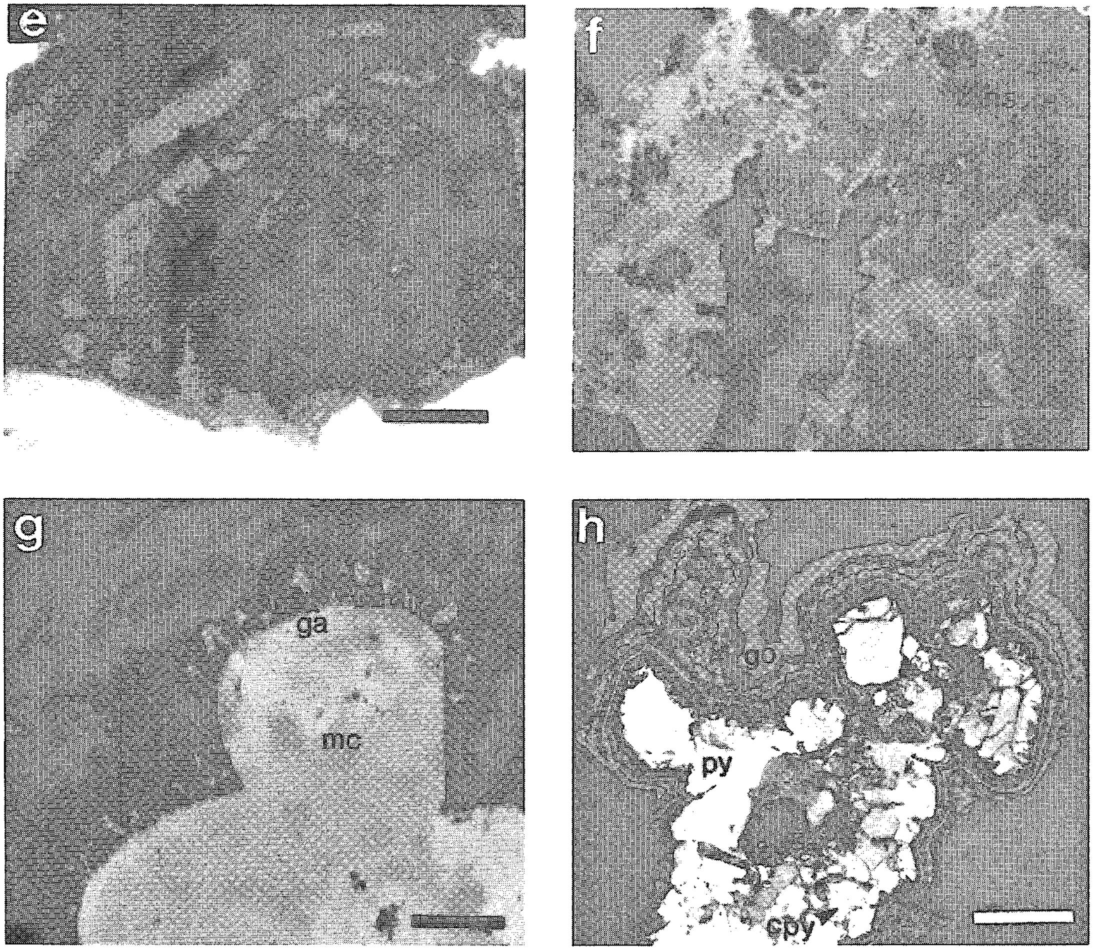

FIG. 3. a–g) Photomicrographs and h) back-scattered electron image of textures in chimney samples 1149–2–18 (21°N) and CY82–31–10 (13°N). a) Chalcopyrite (cpy) exsolution lamellae in isocubanite (ic). Sample 1149–2–18, reflected plane-polarized light, scale bar: 20 μm. b) Dendritic and euhedral pyrite. Sample 1149–2–18, reflected plane-polarized light, scale bar: 60 μm. c) Remnant idiomorphic outlines in pyrite indicating replacement by zinc sulfide. Sample 1149–2–18, reflected plane-polarized light, scale bar: 60 μm. d) Dendritic pyrite overgrown by marcasite (mc). Sample 1149–2–18, reflected cross-polarized light, scale bar: 20 μm. e) Hexagonal grain of wurtzite showing growth zoning. Sample 1149–2–18, transmitted plane-polarized light, scale bar: 50 μm. f) Replacement of zinc sulfide by chalcopyrite along grain boundaries. Sample 1149–2–18, reflected plane-polarized light, scale bar: 20 μm. g) Galena (ga) grains included in zinc sulfide rimming marcasite. Sample 1149–2–18, reflected plane-polarized light, scale bar: 60 μm. h) Colloform goethite (go) rimming pyrite. Sample CY82–31–10, BSE image, scale bar: 60 μm.

Analyses were performed with a 3 MeV proton beam and 6–7 minutes counting time. The 40-μm penetration (Czamanske *et al.* 1993) meant that only those grains larger than 50-μm could be selected for analysis. All analyzed grains were checked for micro-inclusions with a scanning electron-microscope prior to analysis.

DESCRIPTIVE MINERALOGY

Two zoned chimney samples, one from 13°N and one from 21°N, were selected for detailed ore microscopy. Chimney sample CY82–31–10 from Bryce Canyon near 13°N (Fig. 2a) consists of a massive chalcopyrite-rich interior with a rim of bornite. The middle chimney wall is dominated by anhydrite, with disseminated pyrite, chalcopyrite with rare associated isocubanite, and minor magnetite. The exterior wall also is anhydrite-rich, but sulfides are less abundant, and iron oxides (primarily goethite) more abundant in this zone. The 21°N sample (Fig. 2b) also has a chalcopyrite-rich core, but no bornite is present in this chimney. The middle chimney wall is composed predominantly of pyrite with minor zinc sulfide, chalcopyrite and isocubanite, and marcasite. The marcasite content of the chimney increases toward the chimney exterior. Anhydrite is rare in the 21°N chimney, occurring mainly in the chalcopyrite-rich conduit lining.

Chalcopyrite occurs throughout both chimneys, but is most abundant in the central orifice lining, where it forms massive aggregates. Toward the chimney exterior, chalcopyrite is typically associated with zinc sulfide as cavity fillings, chalcopyrite disease (Barton & Bethke 1987), and rims in 1149–2–18, and is interstitial to massive anhydrite in CY82–31–10.

Isocubanite occurs in all parts of chimney sample 1149–2–18 except the interior chalcopyrite-rich zone. It is intimately associated with chalcopyrite, commonly acting as host to micrometric, spindle-shaped exsolution lamellae of chalcopyrite (Fig. 3a) and forming a rim around anhedral grains of chalcopyrite. Rare isocubanite is associated with chalcopyrite in the middle wall of the 13°N sample.

Bornite occurs in the Cu-rich interior of CY82–31–10 as subhedral to anhedral grains interstitial to chalcopyrite. It increases in abundance toward the outside of the chalcopyrite zone until it forms a semicontinuous layer up to 120 μm thick between the chalcopyrite-rich interior and anhydrite-rich exterior zones. Within this bornite-rich zone, some bornite grains contain inclusions of chalcopyrite. Bornite grains are commonly intensely fractured, and the fractures are generally filled with covellite. Bornite is rare in the 21°N chimney, and is associated with chalcopyrite in zinc-sulfide-rich veinlets.

Covellite is intimately associated with bornite in the bornite-rich zone of CY82–31–10. It fills fractures in bornite, but also occurs as anhedral grains interstitial to bornite. Minor covellite occurs in the middle wall of chimney 1149–2–18, associated with chalcopyrite as inclusions or as interstitial anhedral grains.

Pyrite occurs in all zones of both chimneys, but is generally more abundant in the outer zones. Dendritic pyrite is abundant toward the exterior of chimney 1149–2–18, where it is associated with marcasite. Euhedral to subhedral pyrite appears to have formed from dendritic pyrite in some cases (Fig. 3b), and commonly includes grains of zinc sulfide. Euhedral to subhedral grains of pyrite generally occur as cavity and fracture fill in (or as a rim around) zinc sulfide. Atoll textures and remnant idiomorphic outlines of euhedral pyrite (Fig. 3c) indicate replacement of this pyrite by zinc sulfide. In the outermost chimney zone (subsample B), colloform pyrite occurs as spheroidal aggregates commonly forming long branches rimmed by zinc sulfide.

Euhedral to subhedral pyrite grains (<10–50 μm) and granular aggregates occur in cavities in, or

TABLE 2a. MAJOR- AND TRACE-ELEMENT DATA FOR 13°N EAST PACIFIC RISE SAMPLES

		CY82-31 -10a	CY82-31 -10b	CY82-31 -10c	CY82-31 -4a	CY82-31 -4b	CY82-30 -7a	CY82-30 -7b	CY82-21 -3	CY82-30 -2	CY82-31 -7	CY82-31 -9	CY82-31 -3	CY82-31 -5/6
SiO_2	%	nd	0.4	0.3	1.3	1.4	12.0	24.4	1.1	0.1	4.1	0.1	nd	nd
Fe_2O_3		39.5	20.6	26.3	34.6	25.3	45.6	48.4	21.0	24.4	32.8	11.8	47.4	31.8
Na_2O		0.0	0.1	0.1	0.2	0.2	0.1	17.6	20.7	13.0	0.2	24.0	0.3	0.1
Cu		nd	1.2	3.3	0.7	0.2	13.7	4.6	0.4	13.3	0.5	7.6	0.2	nd
S		nd	30.4	31.6	36.3	36.7	32.7	33.6	35.3	28.1	37.8	24.4	nd	nd
Ca		4.1	13.8	14.0	<0.6	<0.1	<0.3	<0.2	<0.2	11.5	<0.4	19.4	nd	nd
Zn		0.1	6.8	4.4	30.5	42.3	<0.1	<0.1	43.0	<0.1	25.6	0.1	8.9	3.3
Pb	ppm	nd	249	139	850	1870	367	479	1660	19	1640	14	875	nd
Ba		75	34	43	bd	90	61	225	267	308	bd	232	bd	bd
W		bd	5	2	bd	bd	bd	bd	bd	6	bd	bd	<2	bd
Mo		bd	28	58	27	15	52	130	34	18	19	158	bd	12
Hg		99	bd	2	2	6	58	24	11	22	6	14	1	1
As		5	68	102	212	166	57	658	3256	195	428	76	371	104
Sb		bd	6	5	22	26	1	3	64	1	15	2	8	4
Br		2	10	6	21	17	25	124	195	103	27	215	33	7
Cr		3	bd	bd	15	3	6	10	9	6	bd	4	bd	11
Ni		bd	bd	bd	bd	bd	62	27	35	139	625	bd	bd	bd
Ag		8	68	35	136	206	4	4	168	15	106	2	48	57
Co		26	168	148	10	66	377	383	4	145	243	59	97	302
Cd		nd	230	152	1110	1060	bd	1	1040	4	650	6	441	202
Bi		nd	<3	<3	5	<3	3	13	<3	<3	<3	<3	nd	nd
Sr		230	7791	bd	1549	8733	bd	127	9572	1035	9962	2062	<134	<242
Mn		<54	34	<35	125	139	<81	<30	154	<66	89	<52	nd	nd
Al		<69500	405	<2024	1647	465	698	1082	992	150	2636	133	nd	nd
In		2.46	6	5.68	19	4.31	<5.0	<1.6	12.2	<4.4	4.68	<2.6	nd	nd
Se		nd	1.1	17	5.6	1.2	480	148	0.2	182	1.8	210	nd	nd
Te		nd	<0.2	0.03	<0.02	<0.02	0.98	<0.02	<0.02	1.48	<0.02	<0.02	nd	nd
Au	ppb	28	412	216	733	1983	56	171	3344	72	1024	68	355	106

interstitial to, anhydrite in zone IV of CY82–31–10. Pyrite may form a rim around chalcopyrite, and replaces chalcopyrite along grain boundaries and fractures. Later chalcopyrite forms a rim on this pyrite. Colloform pyrite is interstitial to anhydrite and is generally surrounded by euhedral pyrite with associated chalcopyrite.

Although *marcasite* occurs throughout the 21°N chimney, it exceeds trace amounts only in the outer zones. Marcasite is most commonly associated with pyrite dendrites, forming subhedral to anhedral overgrowths. Where marcasite occurs with crystalline pyrite, it replaces pyrite inward from grain boundaries (Fig. 3d).

Traces of *pyrrhotite* were observed in the two outermost zones of chimney 1149–2–18. It occurs as small (<10 μm) euhedral prismatic or acicular crystals associated with marcasite.

Both *wurtzite* and *sphalerite* are present in chimney 1149–2–18. Wurtzite was identified by its strong anisotropy in transmitted light and by its hexagonal form. Hexagonal grains commonly are well zoned (Fig. 3e). Where strong anisotropy is not observed, optical distinction between wurtzite and sphalerite is difficult, but X-ray-diffraction patterns do indicate the presence of sphalerite. The term "zinc sulfide" is used where identification is uncertain. Zinc sulfide is most abundant in the middle chimney wall, where it is interstitial to pyrite and occurs as cavity fill or inclusions in pyrite. Toward the chimney interior, zinc sulfide is replaced by chalcopyrite along fractures and grain boundaries (Fig. 3f). Chalcopyrite disease is abundant in zinc sulfide grains that are rimmed by chalcopyrite but absent in unrimmed grains. In the outer chimney walls, the relict cleavage of anhydrite is evidence of replacement of anhydrite by wurtzite.

Traces of *galena* occur in the two outermost zones of chimney 1149–2–18 as small (<10 μm) subhedral inclusions in zinc sulfide rimming marcasite. In some cases, galena grains appear to be radially oriented with respect to the zinc sulfide – marcasite grain boundary (Fig. 3g).

Rare subhedral *magnetite* is disseminated throughout chimney 1149–2–18, generally as individual grains, but also as aggregates. Rare subhedral to anhedral aggregates of magnetite form a rim around sulfides in the 13°N chimney. Magnetite commonly contains grains of pyrite and, more rarely, chalcopyrite. Magnetite in the chimney interior is most commonly associated with chalcopyrite and bornite.

Colloform-banded aggregates of *goethite*, often with pyrite cores, occur in the exterior chimney wall of chimney CY82–31–10 (Fig. 3h).

Anhydrite is present in minor amounts throughout chimney 1149–2–18. In the chimney interior, it occurs as euhedral prismatic crystals interstitial to massive

TABLE 2b. MAJOR- AND TRACE-ELEMENT DATA FOR 21°N EAST PACIFIC RISE SAMPLES

	981R-	981R-	981R-	981R-	981-	1149-2-18				1149-1-1	1149-2-3	1149-2-3	1148-2	1149-1	1149-2	1149-2-18				1150-1
	1-2a	1-2c	2a	2b	R20	A	B	C	D	E	F	G	-6	-1	-3	A1	B1	C1	J	-1
SiO_2 %	9.7	nd	2.2	3.9	1.7	1.1	nd	nd	20.3	nd	nd	nd	2.1	1.1	2.9	nd	nd	nd	nd	2.9
Fe_2O_3	4.6	48.4	40.4	30.2	21.9	44.9	53.8	40	37.8	3.8	24.1	4.4	9.6	4.0	5.8	42.4	34.6	49.8	36.5	12.7
Na_2O	0.3	0.3	0.2	0.4	0.3	0.0	0.1	0	0.1	0.1	0.2	0.1	0.4	0.4	0.2	0.0	0.0	0.0	0.1	0.2
Cu	0.5	nd	20.4	5.9	1.7	23.6	nd	nd	9.4	nd	nd	nd	1.6	1.1	4.1	32.0	5.6	4.2	12.0	1.1
S	20.0	nd	33.8	32.4	28.5	34.2	nd	nd	31.8	nd	nd	nd	24.3	23.6	23.2	nd	nd	nd	nd	29.4
Ca	20.0	11.8	4.8	10.0	8.5	2.1	<0.2	<0.3	<0.3	20.2	11.3	25.0	17.5	23.9	19.6	nd	nd	nd	nd	7.4
Zn	0.1	0.2	0.4	0.7	19.3	0.8	2.4	21.6	8.4	1.6	9.6	0.8	4.8	1.4	3.6	0.2	11.9	10.2	16.1	29.6
Pb ppm	58	nd	86	227	277	69	nd	nd	316	nd	nd	nd	117	42	25	34	477	761	442	390
Ba	68	129	147	79	1715	143	11395	bd	bd	217	103	379	316	212	180	975	651	307	bd	bd
W	bd	2	bd	bd	bd	bd	bd	2	2	bd	2	bd	bd	1	1	bd	9	4	bd	bd
Mo	12	57	49	51	27	28	85	168	147	5	61	5	22	5	10	7	119	99	158	135
Hg	bd	45	60	24	bd	77	bd	31	44	4	22	6	12	5	13	1	3	4	1	11
As	29	178	54	144	51	36	412	384	154	11	150	8	34	7	7	13	204	368	179	185
Sb	1	2	1	3	11	1	17	24	8	1	11	bd	2	1	1	<1	6	12	5	27
Br	14	19	7	8	26	9	6	10	9	10	20	9	34	31	28	5	7	bd	12	25
Cr	bd	15	11	8	bd	6	16	14	15	3	4	3	8	4	12	7	12	19	16	bd
Ni	bd	bd	bd	59	bd	32	56	bd	bd	bd	bd	bd	bd	52	96	bd	bd	bd	bd	bd
Ag	2	26	27	11	39	37	79	44	43	6	29	4	10	3	10	32	35	47	77	42
Co	18	184	168	191	43	206	4	17	198	26	59	28	54	37	75	107	138	90	164	1
Cd	2	nd	20	25	600	34	nd	nd	259	nd	nd	nd	188	58	177	11	698	544	942	789
Bi	bd	nd	bd	59	3	bd	nd	nd	21	nd	nd	nd	6	4	3	nd	nd	nd	nd	bd
Sr	2459	bd	bd	554	bd	bd	bd	bd	142	800	bd	2090	bd	845	bd	bd	bd	bd		7220
Mn	147	486	129	510	283	129	1205	892	330	102	839	104	403	103	187	nd	nd	nd	nd	578
Al	4196	1793	<12316	<2380	1339	<14936	1121	2576	1515	127	<111	247	<642	300	379	nd	nd	nd	nd	7932
In	<0.84	<3.9	3	<1.6	<1.34	4	<0.6	<2.0	<3.62	<0.44	<1.2	<1.5	<0.85	<1.2	<2.1	nd	nd	nd	nd	<0.9
Se	9	nd	390	200	100	501	nd	nd	293	nd	nd	nd	118	33	163	nd	nd	nd	nd	90
Te	1	nd	8	12	4	6	nd	nd	7	nd	nd	nd	1	1	2	nd	nd	nd	nd	<0.02
Au ppb	35	163	49	117	98	48	480	266	97	31	169	29	55	17	25	17	162	364	201	131

Analytical Techniques: SiO_2 Inductively coupled plasma-Mass spectrometry (ICP-MS), Cu and Pb X ray Fluorescence (XRF) and ICP-MS, S LECO, Se and Te Graphite Furnace Atomic absorption (GFAA) Bi and Cd Atomic Absorption (AA), all others by instrumental neutron activation analysis (INAA). nd = not determined, bd = below detection limit chalcopyrite. In outer chimney zones, it is largely replaced by zinc sulfide. In the 13°N chimney, massive anhydrite makes up the central zone, where it is present as large (mm size) tabular crystals.

Traces of *barite* are found in the exterior zones of sample 1149–2–18, where it occurs as acicular crystals associated with marcasite. Barite was not observed in the 13°N chimney.

Amorphous silica occurs as cavity linings, fracture fillings and as a thin (10 μm) rim around the major sulfides of the 21°N chimney, and as cavity fillings in the 13°N chimney.

The mineralogical and textural relationships outlined above are similar to those previously described for chimneys from the East Pacific Rise (Haymon & Kastner 1981, Goldfarb *et al.* 1983, Haymon 1983, Graham *et al.* 1988). In particular, the 13°N chimney shows similarities to the immature chimney type (A) described by Graham *et al.* (1988). Distinguishing characteristics include the presence of bornite, and a high ratio of sulfate to sulfide. Chimneys containing bornite are generally thinner than those without bornite

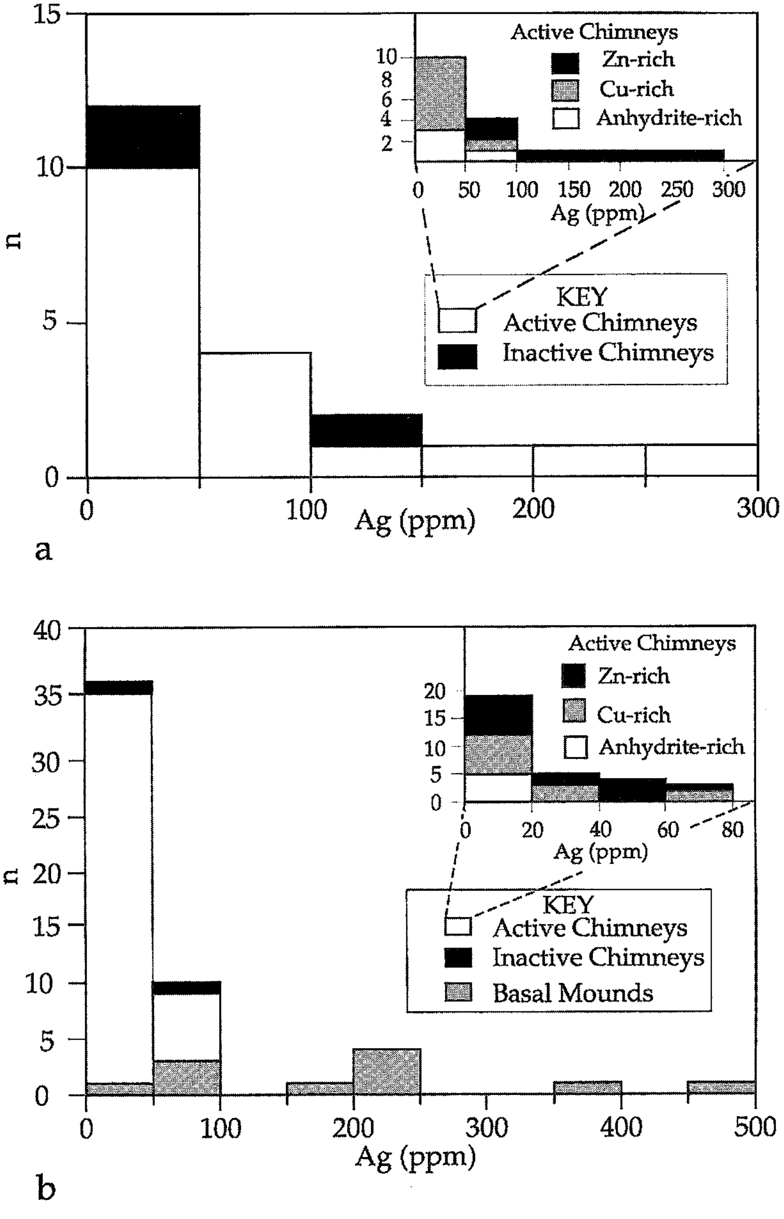

FIG. 4. Distribution of silver in various morphological structures from a) 13°N and b) 21°N, East Pacific Rise. Data from: this study, Bischoff *et al.* (1983), Oudin (1987), Fouquet *et al.* (1988) and Ortega-Osorio & Paez-Osuna (1989).

(Haymon 1983), as is the case of chimney sample CY82–31–10 examined in this study. In contrast to the 13°N sample, chimney sample 1149–2–18 contains no bornite layer, is thicker, and contains a higher ratio of sulfide to sulfate. These specific differences suggest that the 21°N chimney is more mature than the 13°N chimney. Both types of chimney examined bear some similarities to the Cu-rich chimneys described by Goldfarb *et al.* (1983), including a conduit lining of massive coarse-grained chalcopyrite and replacement of zinc sulfides by chalcopyrite.

BULK COMPOSITION

Results of neutron-activation analyses of 33 samples are given in Table 2. The concentration of silver is highly variable, ranging from 2 ppm in sample 981R–1–2a from 21°N to 206 ppm in sample CY82–31–04b from 13°N. Additional data (36 samples) for 21°N from Bischoff *et al.* (1983), Oudin (1987), and Ortega-Osorio & Paez-Osuna (1989) and for 13°N (24 samples) from Fouquet *et al.* (1988) indicate a range of silver contents from 0 up to 464 ppm. Zinc-rich chimneys from 13°N (Fig. 4a) have up to three times the silver content of similar chimneys at 21°N (Fig. 4b). At 21°N, silver is more abundant in samples from basal mounds than it is in either active or inactive chimneys (Fig. 4b). Linear correlation-coefficients (significant at the 95% level) are positive between Ag and Pb, S, Sb, Cd, Mn and Au at both 21°N and 13°N (Fig. 5). A negative correlation exists between Ag and Ca in both areas, which is a result of an inverse relationship between the silver and anhydrite contents of the hydrothermal chimneys

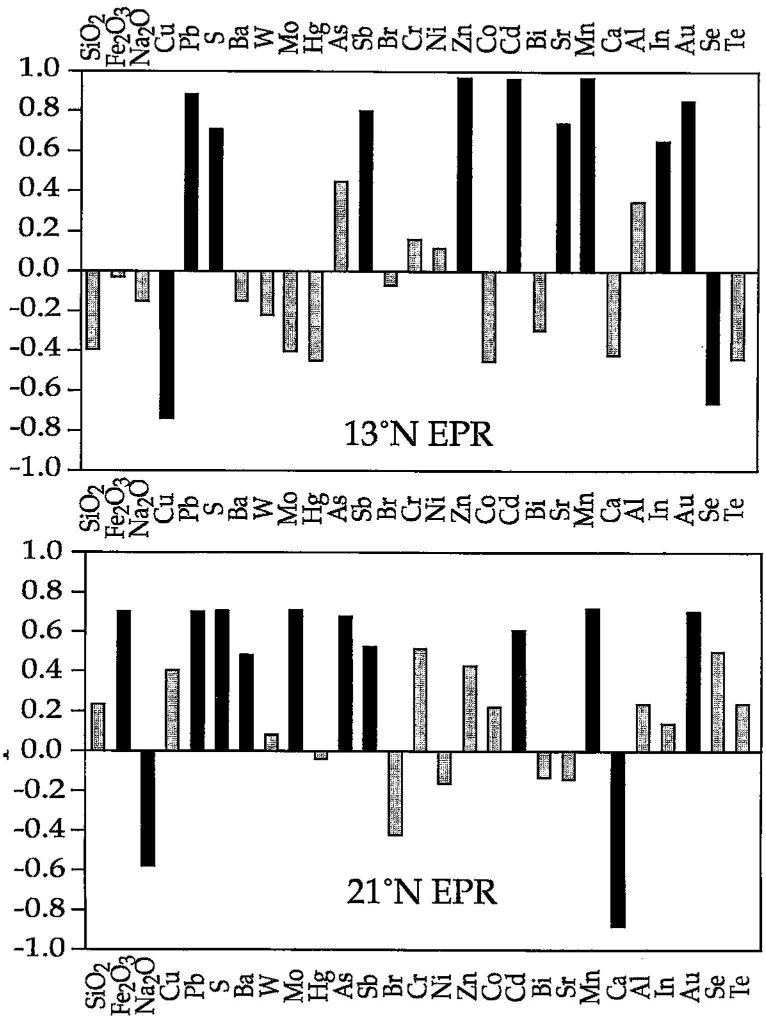

FIG. 5. Correlation coefficients (r) of Ag and other elements for bulk chemical analysis of samples from 13°N and 21°N, East Pacific Rise. (Black bars represent coefficients significant at the 95% level).

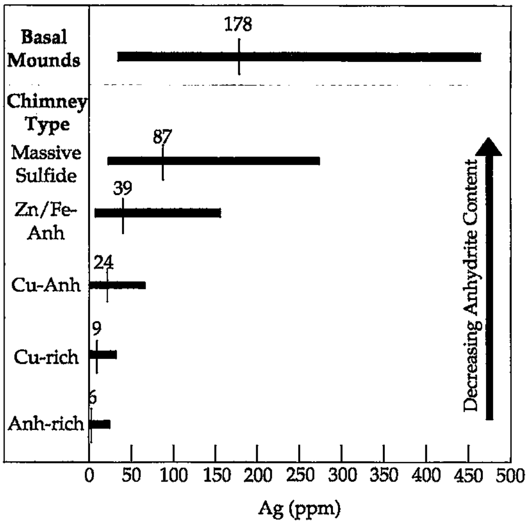

FIG. 6. Silver content (range and mean) of chimneys from 21°N and 13°N, East Pacific Rise, and basal mounds from 21°N. Anh: anhydrite. Sources: This study, Bischoff *et al.* (1983), Oudin (1987), Fouquet *et al.* (1988) and Ortega-Osorio & Paez-Osuna (1989).

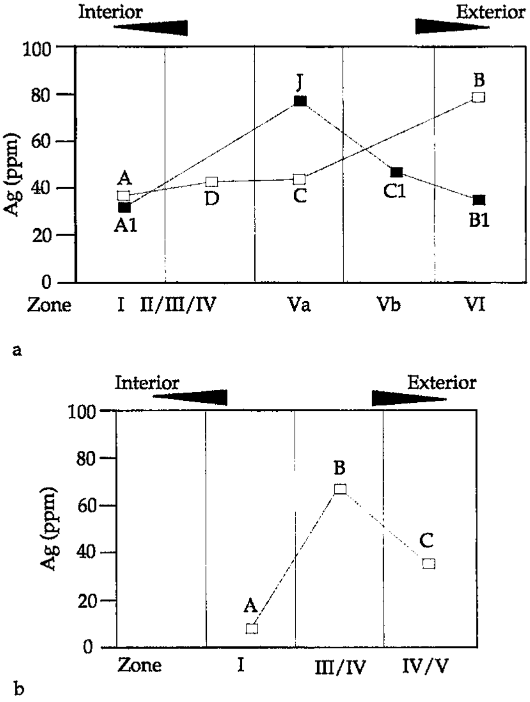

FIG. 7. Distribution of silver in cross sections through black smoker chimneys. a) Two profiles (A–B and A1–B1) through 1148–2–18, 21°N, and b) CY82–31–10, 13°N East Pacific Rise. See Figure 2 for description of zones and location of subsamples.

(Fig. 6). The chimneys with higher contents of anhydrite tend to contain less Ag (average 6 ppm) than those composed of predominantly massive sulfide (average 87 ppm). Basal mounds, from which most of the anhydrite has been dissolved during the construction process, have an even higher average content of silver, 178 ppm.

Analyses of subsamples of zoned chimneys 1149–2–18 (21°N) and CY82–31–10 (13°N) reveal two trends of silver distribution in the chimney cross-sections (Fig. 7). In one profile (A1–B1) of 1149–2–18, silver is concentrated in the middle zone (Va), and in the other profile, it is concentrated in the exterior chimney wall (Fig. 7a). As, Au, Mn, Zn, Sb and Mo are enriched in the middle chimney wall (Moss & Scott 1994). Results for chimney sample CY 82–31–10 from 13°N are shown in Figure 7b. The silver content is highest in the middle anhydrite-rich zone and drops off to approximately half that level in the outermost zone, in a similar manner to profile A1–B1 of the 21°N sample. Au, Sb and Zn are also enriched in the middle zone (Moss & Scott 1994).

COMPOSITION OF THE MINERALS

The composition of individual sulfides from the 21°N and 13°N chimney samples are summarized in Table 3.

Cu–Fe sulfides

EMPA of chalcopyrite grains from the conduit lining of sample 1149–2–18 show the silver content to vary from <100 to 900 ppm. Chalcopyrite also contains up to 5000 ppm Zn, 500 ppm Co and 1400 ppm Hg.

TABLE 3. SILVER CONTENT OF SULFIDES FROM EAST PACIFIC RISE CHIMNEYS

	21°N 1149-2-18				13°N CY82-31-10
Electron Microprobe Sub-sample	A	B	C	D	3
cpy	nd	nd	nd	<100-900 (462)	<100-700(250)
icb	no	nd	nd	<100-500 (283)	nd
ZnS	all<200	<200-2990 (396)	<200-200 (112)	<200-300 (114)	nd
py	nd	nd	nd	nd	<100-200 (80)
mc	no	nd	nd	nd	nd
ga	no	4800-9500 (7270)	<4400-8100 (3780)	no	no
Proton Microprobe Sub-sample	A1	B1	C1	J	
cpy	32-49 (37)	364,476	247-279 (265)	41-240 (183)	
ZnS	no	<6-16 (8)	6-188 (63)	<6-80 (37)	
py	5-35 (13)	8-40 (18)	nd	10-162 (89)	
mc	no	21,103	14,43	nd	
py/mc	nd	nd	19-59 (36)	168	

Range (mean) values in ppm; means are calculated assuming values below detection are equal to half the detection limit. Detection limits for Ag by EMPA are: cpy, icb and py: 100 ppm, ZnS: 200 ppm, and ga: 4400 ppm. Detection limits for Ag by PMPA are: cpy: 5 ppm, ZnS: 6 ppm, and py and mc: 4 ppm. nd = not determined, no = mineral not observed. Abbreviations: cpy chalcopyrite, ga galena, icb isocubanite, mc marcasite, py pyrite, py/mc intergrown pyrite and marcasite, ZnS zinc sulfide. Subsamples are located in Figure 6.

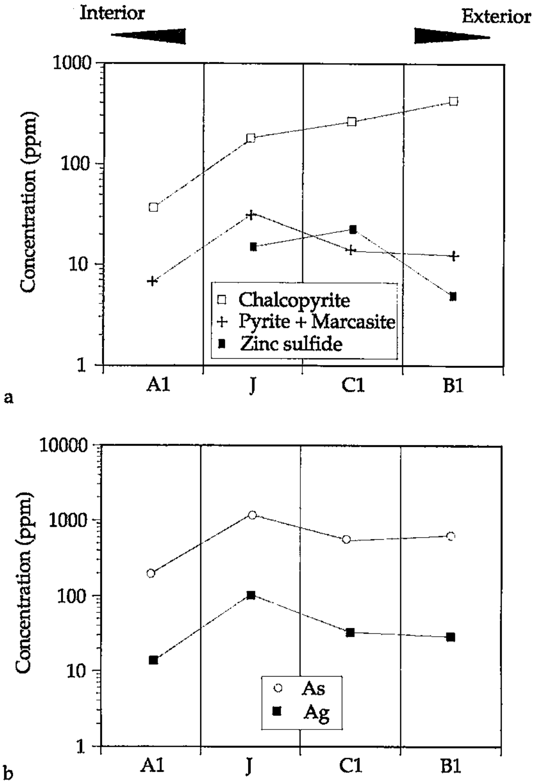

FIG. 8. a) Silver variation in sulfides through zoned chimney sample 1149–2–18 from 21°N East Pacific Rise. b) As and Ag in pyrite and marcasite in chimney sample 1149–2–18. Descriptions and locations of subsamples A1, J, C1 and B1 are in Table 1 and Figure 2, respectively.

Isocubanite from the same sample has higher Zn and Co contents and lower Hg contents, with a maximum silver content of 500 ppm. Proton-microprobe results for chalcopyrite (Fig. 8a) indicate a progressive increase in silver content from the interior chalcopyrite-rich zone (average: 37 ppm) to the exterior chimney wall (average: 420 ppm). Massive chalcopyrite from the interior of chimney sample CY82–31–10 (13°N) has a range of silver contents from <100 to 700 ppm (EMPA). In addition, up to 800 ppm Co and 800 ppm Hg are present in the chalcopyrite.

Fe sulfides

The silver content of pyrite determined by proton microprobe is highest in subsample J of chimney sample 1149–2–18 (Fig. 8a). The silver contents of the innermost and outermost zones are statistically indistinguishable, with averages of 13 and 18 ppm, respectively. The Ag content of marcasite is similar to that of pyrite, ranging from a low of 14 ppm in subsample C1 to a high of 103 ppm in the outermost zone. The variations in the silver contents of pyrite and marcasite through the chimney are closely matched by a variation in As content (Fig. 8b). Electron-microprobe analyses of pyrite at 13°N indicate that Ag, where present, is generally at levels below the detection limit (100 ppm).

Zn sulfides

Proton-microprobe analyses of zinc sulfides show silver to be concentrated in subsample C1 (Fig. 8a), in which these minerals are most abundant. Proton-microprobe values for Ag were generally found to be less than those obtained by electron microprobe; those values, as high as 3000 ppm, presumably reflect the presence of inclusions that were not resolved optically.

The iron content of zinc sulfide from sample 1149–2–18 is shown in Figure 9. It is most variable in the exterior wall (subsample B), where values of mol.% FeS range from a low of 7 to a high of 34. Zinc sulfides with the highest iron contents are typically found as inclusions in pyrite, an observation previously reported by Hekinian *et al.* (1980). Subsample C has the highest average value, 21 mol.% FeS, corresponding to the value for the pyrite–pyrrhotite buffer (Scott & Barnes 1971). The chimney interior (subsample A) shows significantly lower mol.% FeS (average: 3.2) in zinc sulfides coexisting with chalcopyrite. Results of 137 electron-microprobe analyses of zinc sulfide failed to indicate any significant correlation between FeS and silver content. This is in contrast to the findings of Zierenberg *et al.* (1984), who found silver to be preferentially concentrated in low-Fe zinc sulfide. There is also no significant correlation between mol.% FeS in zinc sulfide and bulk silver content as determined by INAA.

Reaction-path modeling of a Southwest vent fluid demonstrates that the sulfur fugacity of pore fluid decreases slightly from the interior to the exterior across a chimney wall (Tivey & McDuff 1990). Sulfur activity in chimney sample 1149–2–18 estimated from mol.% FeS of zinc sulfide (Scott 1983) in Figure 9, is lowest in subsample C and highest in the exterior chimney wall (subsample B). The estimates of sulfur activities range from $10^{-8.0}$ to $10^{-9.3}$ for the 349°C temperature of the Southwest vent fluid.

Galena

Of eight electron-microprobe analyses of galena from sample 1149–2–18, Ag is below the detection limit (MDL: 0.44 wt%) in three, and has a high value of 0.95% in subsample B from the outermost zone of the chimney. The average silver content of galena

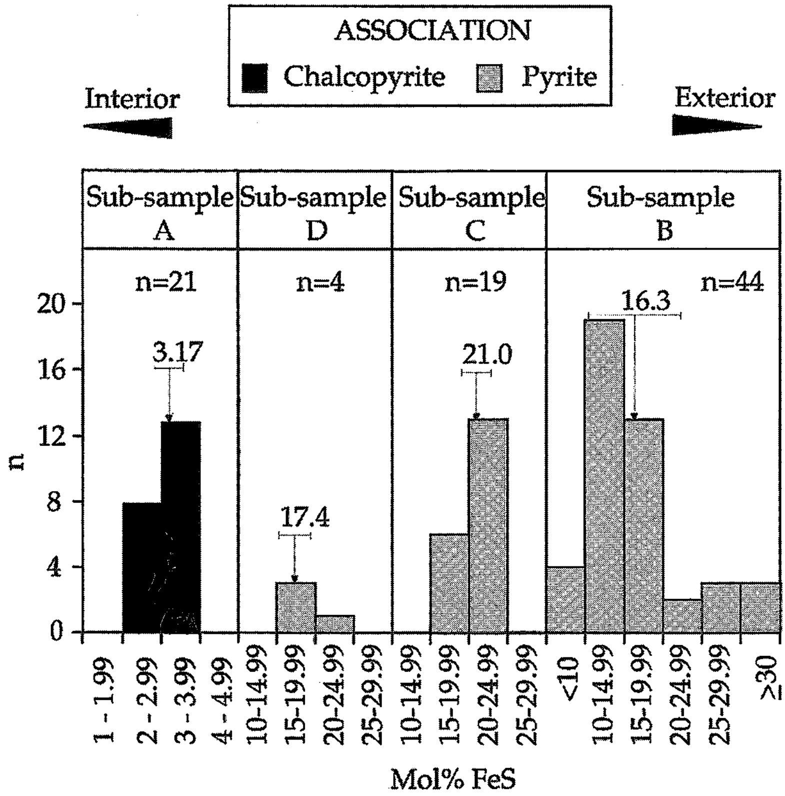

FIG. 9. Frequency distributions of mol.% FeS in zinc sulfide through chimney sample 1149–2–18, 21°N East Pacific Rise. Mean and standard deviation are indicated; n: number of analyses.

almost doubles from 3780 ppm in the chimney interior to 7270 ppm in the outermost zone. High values of silver are accompanied by high values of antimony (a significant correlation at the 95% level), the presence of which is known to increase the solubility of silver in galena (Amcoff 1976, 1984, Sharp & Buseck 1993).

The contribution by individual minerals to the bulk silver content of chimney sample 1149–2–18 was calculated using modal percentages determined by image analysis supplemented by point counting. All of the silver obtained by INAA is accounted for by the silver content of the major sulfides (Table 4). A separate silver sulfide or sulfosalt is not indicated. Chalcopyrite, pyrite and marcasite contribute most of the silver in all but subsample C1, where the major contribution is made by zinc sulfide. Galena, which contains the highest amounts of silver of all sulfides analyzed, does not make a significant contribution owing to its low abundance.

TABLE 4. MINERALOGICAL CONTRIBUTION TO THE BULK SILVER CONTENT OF CHIMNEY SAMPLE 1149-2-18

	Subsample A1			Subsample J		
Phase	Modal %	contribution ppm	1σ	Modal %	contribution ppm	1σ
Zinc Sulfide	0.8	0.0	3	25.1	8.5	2
FeS_2 (total)	6.2	1.1	1	24.3	35.3	14
Pyrite	6.2			19.0		
Marcasite	0.0			5.3		
Chalcopyrite	67.5	30.6	7	26.6	58.0	33
Silica	8.3			8.6	nd	
Sulfate	4.1			0.0	0.0	
Porosity	13.0			15.5	0.0	
Total	99.9	31.7	11	100.1	101.8	49

	Subsample C1			Subsample B1		
Phase	Modal %	contribution ppm	1σ	Modal %	contribution ppm	1σ
Zinc Sulfide	34.7	29.4	7	4.0	0.6	2
FeS_2 (total)	27.1	14.2	4	31.5	19.3	12
Pyrite	18.5			14.7		
Marcasite	8.6			16.8		
Chalcopyrite	2.8*	8.7		2.0	17.6	16
Silica	5.8	nd		18.2	nd	
Sulfate	0.0	nd		0.0	nd	
Porosity	29.5	0.0		44.2	0.0	
Total	99.9	52.3	11	99.9	37.5	30

Modal % determined by image analysis except pyrite, marcasite and * determined by point counting. Mineralogical contribution is calculated from modal % and proton microprobe analyses. 1σ represents the error in the mineralogical contribution. Abbreviation: nd = not determined.

FLUID CHEMISTRY

The compositions of end-member vent fluids (Table 5) were calculated for fluids sampled from the chimney from which sample 1149–2–18 was taken (Von Damm 1983), and in the vicinity of Bryce Canyon, 13°N (Michard *et al.* 1984, Bowers *et al.* 1988). Because there is no Mg in end-member hydrothermal fluids, end-member compositions correspond to the zero Mg intercept in a linear regression for the element of interest *versus* Mg (Von Damm 1983, Bowers *et al.* 1988). The calculated concentration of chloride in the Southwest fluid (495 mmol/kg) is slightly lower than that of seawater (541 mmol/kg), whereas the chloride content of the 13°N fluid (776 mmol/kg) is greater. Such enrichments and depletions of chloride relative to seawater have been explained by Von Damm (1988, 1990) in terms of mixing of modified seawater, brine, and vapor. Phase separation prior to mixing results in formation of a chloride-depleted vapor and a chloride-enriched brine. Modified seawater does not undergo phase separation, and thus contains normal amounts of chloride.

TABLE 5. FLUID CHEMISTRY FROM EAST PACIFIC RISE VENTS

		13°N near Bryce Canyon	21°N South West (SW2) Vent	Seawater
Temp.	°C	320	349	2
$pH_{(Temp.)}$		2.1	3.5	7.2
alk	meq	-0.7*	-0.3	2.3
Cl	mmol/kg	775.6	494.9	541
Br	mmol/kg	1.2	nd	0.84
SiO_2	mmol/kg	23.7	17.4	0.16
Al	mmol/kg	15.2	6.3	0.02
Li	mmol/kg	767.7	904.1	26
Na	mmol/kg	630.2	436.0	464
K	mmol/kg	30.5	23.5	9.8
Rb	mmol/kg	14.0	27.7	1.3
Mg	mmol/kg	0.0	0.0	52.7
Ca	mmol/kg	54.9	16.5	10.2
Sr	mmol/kg	187.0	84.4	87
Ba	mmol/kg	nd	5.5	0.14
SO_4	mmol/kg	0.0	0.6	27.9
H_2S	mmol/kg	8.2*	7.1	0.0
Mn	mmol/kg	1278.2	761.5	<0.001
Fe	mmol/kg	1842.3	740.1	<0.001
Co	nmol/kg	nd	62.0	0.03
Cu	mmol/kg	nd	9.0	0.007
Ag	nmol/kg	nd	22.1	0.02
Zn	mmol/kg	5*	78.9	0.01
Cd	nmol/kg	70*	131.6	1.0
Pb	nmol/kg	27*	173.1	0.01
As	nmol/kg	nd	177.2	27

End–member–fluid chemistry for 13°N calculated from data of Michard *et al.* (1984) except * from Bowers *et al.* (1988). Data for 21°N calculated from Von Damm (1983). Seawater data from Von Damm (1990). nd: not determined.

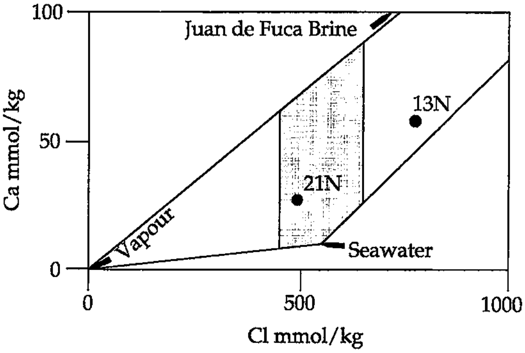

FIG. 10. Three-component mixing model with 21°N and 13°N fluids plotted (modified from Von Damm 1988). The shaded area represents the field in which the fluid characteristics are determined by basalt–fluid interaction alone. The composition of the Juan de Fuca brine (3.27 mol/kg Cl and 441 mmol/kg Ca: Von Damm 1988) lies off the diagram in the direction of the arrow.

Figure 10 is a plot of calcium against chloride for East Pacific Rise fluids in terms of this three-component mixing model. Both the 13°N and 21°N fluids plot in the field of three-component mixing, but the composition of the 21°N fluid can be explained by mineralogical control alone, whereas the area in which the 13°N fluid plots suggests addition of brine to the modified seawater.

DISCUSSION

Transport and deposition of silver in the 21°N fluid

Published data on mid-ocean ridge hydrothermal fluids indicate concentrations of silver at the ppb level (Von Damm *et al.* 1985a, b). At 21°N, East Pacific Rise, the concentration of silver is greatest in the OBS and HG vent fluids (38 and 37 nmol/kg, respectively), and below detection (<1 nmol/kg) in NGS fluids (Von Damm *et al.* 1985a). Fluid venting at the Southwest (SW2) site contains 22 nmoles/kg (~2 ppb) silver, a 10^3 enrichment over the 20 pmoles/kg Ag in seawater (Von Damm 1990).

Several experimental investigations have demonstrated the relative importance of different complexes of silver under various conditions. Bisulfide complexes (Sugaki *et al.* 1987, Gammons & Barnes 1989) and chloride complexes (Seward 1976, Zotov *et al.* 1986a, Levin 1992, Gammons & Williams-Jones 1994, 1995) have been studied the most, but carbonate (Kozlov 1985), hydroxy (Kozlov *et al.* 1983), and hydroxychloride (Zotov *et al.* 1982) complexes and the aqueous form of the silver ion (Zotov *et al.* 1986b) also have been considered. Hydroxychloride and hydroxy complexes of silver and Ag^o_{aq} are stable only in very alkaline solutions, which are unlikely to exist under normal hydrothermal conditions (Zotov *et al.* 1982, Kozlov *et al.* 1983, Kozlov & Khodakovskiy 1983). Carbonate complexes are unlikely silver carriers, especially at high temperatures, owing to their narrow fields of stability (Kozlov 1985). In a study of Ag_2S solubility in sulfide solutions, Sugaki *et al.* (1987) found that dissolution of Ag_2S results in the formation of dinuclear complexes such as $Ag_2S(H_2S)$, which is the predominant dinuclear species at temperatures greater than about 200°C. Gammons & Barnes (1989) determined $Ag(HS)_2^-$ to be the stable bisulfide complex under similar conditions, and suggested that mononuclear species are more likely to be stable than dinuclear species. Both the mononuclear $Ag(HS)_2^-$ and the dinuclear $Ag_2S(H_2S)$ species are considered here as possible complexes.

Calculated fields of stability of chloride and bisulfide complexes of silver for conditions in the Southwest vent fluid are shown in Figure 11. Very high activity of H_2S favors formation of the dinuclear $Ag_2S(H_2S)$ complex. $Ag(HS)_2^-$ and eventually Ag^+ become the predominant aqueous species as sulfur activity decreases. Increasing activity of chloride ion results in formation of chlorosilver complexes with progressively greater coordination numbers.

Speciation of the Southwest 2 (SW2) end-member fluid composition (Table 5) was calculated using the SOLMINEQ88 code (Perkins *et al.* 1989), and gave the following results for a fluid temperature of 349°C (corresponding to the average temperature of the SW2 fluid during sample collection): $a(Cl^-) = 0.09$, $a(H_2S) = 0.009$, pH = 4.6, $a(SO_4^{2-}) = 8.2 \times 10^{-7}$ and $a(O_2) = 4.5 \times 10^{-27}$. The calculated values of $a(Cl^-)$ and $a(H_2S)$ for the SW2 fluid plot in the $AgCl_2^-$ field (Fig. 11), indicating transport of silver as this chlorocomplex. Calculations of stability of the silver complex show that 1) silver transported as the $AgCl_2^-$ complex can account for all the measured silver in the fluid, and 2) silver in the fluid is undersaturated with respect to Ag_2S (Table 6).

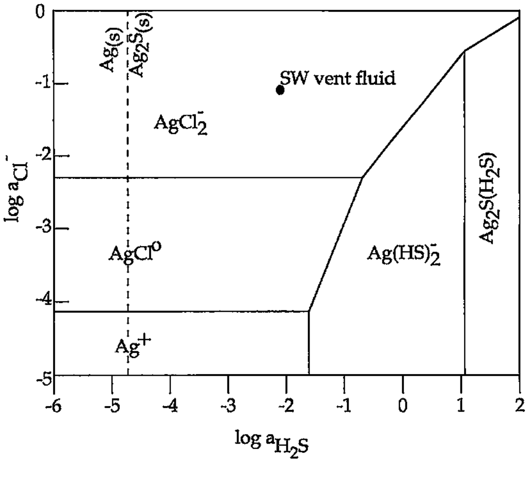

FIG. 11. Predominance-area diagram of silver complexes as a function of Cl^- and H_2S activity. Temperature = 350°C, pH = 4.6, log $a(O_2) = -26.4$. Sources of data: composition of Southwest fluid calculated from data of Von Damm (1983); solubility data from Gammons & Barnes (1989), Seward (1976), and Sugaki *et al.* (1987); additional data from Johnson *et al.* (1992).

TABLE 6. CALCULATED SATURATION VALUES AND CONCENTRATIONS OF SELECTED METALS AS CHLORIDE COMPLEXES IN A 21°N VENT FLUID

Metal	Calculated[1] $\times 10^{-6}$moles/kg	Analyzed[2] $\times 10^{-6}$moles/kg
ΣAg	15,240	0.0221
ΣPb	540	0.1731
ΣZn	113,300	78.900

Data Sources: 1 Seward (1976, 1984), Ruaya & Seward (1986); 2 Von Damm (1983). Calculated values are for all Ag as $AgCl_2^-$, $\Sigma Pb = PbCl_2^\circ + PbCl_3^-$, and $\Sigma Zn = ZnCl_2^\circ + ZnCl_3^-$.

Precipitation of metals from solution takes place in response to changing physicochemical conditions at the site of deposition. Precipitation of Ag carried as the dichlorosilver complex can be represented by:

$$2AgCl_2^- + H_2S = Ag_2S + 2H^+ + 4Cl^- \qquad (1)$$

Equation 1 indicates that increasing pH, $a(H_2S)$ and decreasing activity of chloride ion will favor an increase in the saturation index (log IAP/Ksp, where IAP is the ion-activity product and Ksp is the solubility product) of Ag in the fluid or, if carried far enough, precipitation of silver as Ag_2S. Decreasing temperature also will increase the saturation index of Ag. Models for the mixing of seawater and hydrothermal fluids from 21°N (Bowers *et al.* 1985, Tivey & McDuff 1990) indicate that pH increases as the temperature decreases from 350° to about 25°C, approaching the value for seawater at low temperatures. Mixing of hydrothermal fluid with seawater can therefore provide the necessary conditions for effective precipitation of silver as Ag_2S.

The silver content of the Southwest hydrothermal fluid is, however, clearly undersaturated with respect to Ag_2S (Table 6). Although the reaction path as modeled by Bowers *et al.* (1985) predicts the formation of acanthite as the stable silver phase, none has been observed at 21°N. Neither have any other discrete silver minerals been reported from 21°N, suggesting that silver remains undersaturated with respect to Ag_2S

under all conditions at 21°N. The silver content of chimney 1149–2–18 has been accounted for by its concentration in major sulfides at all stages of the paragenesis (Table 4). Silver was therefore partitioned into precipitating sulfides rather than forming discrete silver minerals. The actual form that the silver has in the sulfides is not known, but investigations of the silver content of sulfides from ancient VMS deposits indicate that silver may occur as structurally bound silver, colloidal-size silver, or submicroscopic inclusions (Laroque *et al.* 1995).

Models of chimney growth

The concentration of silver in chimney samples 1149–2–18 and CY82–31–10 has been shown to be highest within the middle to outer chimney walls, and, more generally, to increase with decreasing content of anhydrite. Both of these observations can be related to the growth of hydrothermal chimneys. Models of black-smoker chimney growth (Haymon 1983, Turner & Campbell 1987, Graham *et al.* 1988, Tivey & McDuff 1990) suggest that chimneys initially grow upward and outward by precipitation of anhydrite at the fluid–seawater interface. This first stage of growth results in an anhydrite-rich chimney of more or less uniform porosity. As growth continues, hydrothermal fluid in the central conduit is insulated from the surrounding seawater owing to precipitation of anhydrite and sulfides in the middle chimney wall. Such precipitation allows high-temperature Cu–Fe sulfides to precipitate on the interior wall, with resultant growth of the chimney into the central orifice. The anhydrite content of the chimney is gradually reduced by dissolution at the chimney–seawater interface, and by replacement by sulfides within the chimney. The observed inverse relationship between silver concentration and anhydrite content is thus a function of chimney maturity, with mature anhydrite-poor chimneys containing more silver than immature anhydrite-rich chimneys. Further evidence for a relationship between silver concentration and maturity is found in the silver content of basal mounds. Such mounds, formed in part from the coalescence of collapsed chimneys, represent the most mature morphological features of a particular system, and are generally richer in silver than are chimneys (Fig. 4b).

Two mechanisms of cooling have been considered for hydrothermal chimneys (Bowers *et al.* 1985): 1) conductive cooling, by which heat escapes through the chimney wall into the surrounding water, and 2) mixing of hydrothermal fluid and seawater within the chimney walls. Cooling by mixing is expected to be important early in the life of the chimney owing to the available porosity, which allows the seawater and hydrothermal fluid to mix. This kind of cooling should form well-zoned chimneys with mineral and textural zones reflecting different physicochemical regimes (Bowers *et al.* 1985, Tivey & McDuff 1990). Conductive cooling may become more important later, as precipitation of minerals in pore spaces within the chimney walls reduces porosity, and chimneys become plugged. An example of late conductive cooling is given by Campbell *et al.* (1988), who reported a chimney from the NGS vent field that in 1979 was a 350°C black smoker, but which had become inactive by 1981. When this chimney was broken open, it vented 273°C fluid and became a white smoker. It appears therefore that this particular chimney was undergoing conductive cooling before being broken open. Of these two mechanisms of cooling, fluid–seawater mixing is likely to be the more effective means of silver precipitation, owing to larger gradients of temperature, pH and $a(O_2)$. Conductive cooling is expected to produce small-scale local precipitation of metals from trapped pore fluid. Overall enrichment of silver in the middle and outer parts of active chimneys 1149–2–18 and CY82–31–10 suggests that silver is preferentially deposited in the cooler parts of the chimney, where there is a higher ratio of seawater to hydrothermal fluid.

CONCLUSIONS

Silver in the Southwest hydrothermal fluid is present at the ppb level, is shown to be transported predominantly as the $AgCl_2^-$ complex, and is undersaturated with respect to Ag_2S. The lack of discrete silver minerals in East Pacific Rise chimneys suggests that silver remained undersaturated during the chimney-building process.

Bulk silver contents of subsamples from chimney sample 1149–2–18 can be accounted for by incorporation in major sulfides. Galena generally has the highest average values of silver, followed by chalcopyrite, isocubanite, zinc sulfide, pyrite and marcasite. The silver content of chalcopyrite is, however, strongly dependent on position in the chimney wall, being lowest in chalcopyrite from the conduit lining, and highest in chalcopyrite in the outer wall. This mineralogical control affects the bulk distribution of silver within chimneys. The lowest concentrations of silver are found in the Cu–Fe sulfide-rich interior wall of the chimney, the site of the highest-temperature precipitation.

The bulk silver contents of chimneys from 21°N and 13°N, East Pacific Rise are highly variable; they range from a low of 2 ppm to a high of 206 ppm. This variability is due in part to a strong positive correlation between the Ag content of a chimney and the chimney's maturity, such that silver concentration increases throughout the chimney's lifetime. Silver concentration is also generally higher in basal mounds. These have formed by the coalescence of collapsed chimneys, and thus represent the most mature morphological structures. A similar relationship between maturity and concentration exists for Au (Hannington & Scott 1989). The interplay of the stability of chloride and sulfide complexes of Ag and Au, both of which are highly undersaturated in vent fluids, may be responsible for the observed greater than ten-fold variability of Au:Ag ratio (Hannington *et al.* 1991) in seafloor deposits.

ACKNOWLEDGEMENTS

We are grateful to Yves Fouquet of IFREMER for providing the samples from 13°N, and to John Edmond of Woods Hole Oceanographic Institute for providing the 21°N samples. Thanks to Greg Anderson and Ed Spooner for reading and suggesting improvements to an earlier version of this manuscript. The thoughtful comments of referees P. McGoldrick and S. Larocque, and Associate Editor R.R. Keays, and the thorough editing of R.F. Martin, further improved the manuscript. Claudio Cermignani, Neil Coombs, Michael Gorton, Ron Hancock and Susan Aufreiter assisted with various analytical techniques. John Rucklidge introduced RM to image analysis. Bill Teesdale and Iain Campbell of the University of Guelph are thanked for their assistance with the proton-microprobe analyses. The research was funded by the Natural Sciences and Engineering Research Council of Canada and the Bank of Nova Scotia through grants to SDS and by the University of Toronto through an Open Fellowship to RM.

REFERENCES

Amcoff, Ö. (1976): The solubility of silver and antimony in galena. *Neues Jahrb. Mineral., Monatsh.*, 247-261.

——— (1984): Distribution of silver in massive sulfide ores. *Mineral. Deposita* **19**, 63-69.

Ballard, R.D. & Francheteau, J. (1982): The relationship between active sulfide deposition and the axial processes of the mid-ocean ridge. *Marine Tech. Soc. Bull.* **16**, 8-22.

———, ———, Juteau, T., Rangan, C. & Normark, W. (1981): East Pacific Rise at 21° N: the volcanic, tectonic and hydrothermal processes of the central axis. *Earth Planet. Sci. Lett.* **55**, 1-10.

———, Hekinian, R. & Francheteau, J. (1984): Geological setting of hydrothermal activity at 12°50′N on the East Pacific Rise: a submersible study. *Earth Planet. Sci. Lett.* **69**, 176-186.

Barton, P.B., Jr. & Bethke, P.M. (1987): Chalcopyrite disease in sphalerite: pathology and epidemiology. *Am. Mineral.* **72**, 451-467.

Bischoff, J.L., Rosenbauer, R.J., Aruscavage, P.J., Baedecker, P.A. & Crock, J.G. (1983): Sea-floor massive sulfide deposits from 21°N, East Pacific Rise; Juan de Fuca Ridge; and Galapagos Rift: bulk chemical composition and economic implications. *Econ. Geol.* **78**, 1711-1720.

Bowers, T.S., Campbell, A.C., Measures, C.I., Spivack, A.J., Khadem, M. & Edmond, J.M. (1988): Chemical controls on the composition of vent fluids at 13°N–11°N and 21°N, East Pacific Rise. *J. Geophys. Res.* **93**, 4522-4536.

———, Von Damm, K.L. & Edmond, J.M. (1985): Chemical evolution of mid-ocean ridge hot springs. *Geochim. Cosmochim. Acta* **49**, 2239-2252.

Cabri, L.J., Harris, D.C. & Nobiling, R. (1984): Trace silver analyses by proton microprobe in ore evaluation. *In* Precious Metals: Mining, Extraction and Processing (V. Kudryk, D.A. Corrigan & W.W. Liang, eds.). Metall. Soc. AIME Proc., 93-100.

Campbell, A.C., Bowers, T.S., Measures, C.I., Falkner, K.K., Khadem, M. & Edmond, J.M. (1988): A time series of vent fluid compositions from 21°N, East Pacific Rise (1979, 1981, 1985), and the Guaymas Basin, Gulf of California (1982, 1985). *J. Geophys. Res.* **93**, 4537-4549.

Chryssoulis, S.L. & Surges, L.J. (1988): Behaviour of terahedrite in the mill circuits of Brunswick Mining and Smelting Corporation, Ltd. *In* Silver – Exploration, Mining & Treatment. Inst. Mining Metall., 205-216.

Czamanske, G.K., Sisson, T.W., Campbell, J.L. & Teesdale, W.J. (1993): Micro-PIXE analysis of silicate reference standards. *Am. Mineral.* **78**, 893-903.

Fouquet, Y., Auclair, G., Cambon, P. & Etoubleau, J. (1988): Geological setting and mineralogical and geochemical investigations on sulfide deposits near 13°N on the East Pacific Rise. *Marine Geol.* **84**, 145-178.

Francheteau, J., Needham, H.D., Choukroune, P., Juteau, T., Séguret, M., Ballard, R.D., Fox, P.J., Normark, W., Carranza, A., Cordorba, D., Guerrero, J., Rangin, C., Bougault, H., Cambon, P. & Hekinian, R. (1979): Massive deep-sea sulphide ore deposits discovered on the East Pacific Rise. *Nature* **277**, 523-528.

Gammons, C.H. & Barnes, H.L. (1989): The solubility of Ag_2S in near-neutral aqueous sulfide solutions at 25 to 300°C. *Geochim. Cosmochim. Acta* **53**, 279-290.

——— & Williams-Jones, A.E. (1994): Solubility of Au–Ag alloys in hydrothermal brines. *Geol. Assoc. Can. – Mineral. Assoc. Can., Program Abstr.* **19**, A39.

——— & ——— (1995): Hydrothermal geochemistry of electrum: thermodynamic constraints. *Econ. Geol.* **90**, 420-432.

Gente, P., Auzende, J.M., Renard, V., Fouquet, Y. & Bideau, D. (1986): Detailed geological mapping by submersible of the East Pacific Rise axial graben near 13°N. *Earth Planet. Sci. Lett.* **78**, 224-236.

GOLDFARB, M.S., CONVERSE, D.R., HOLLAND, H.D. & EDMOND, J.M. (1983): The genesis of hot spring deposits on the East Pacific Rise, 21°N. *In* The Kuroko and Related Massive Sulfide Deposits (H. Ohmoto & B.J. Skinner, eds.). *Econ. Geol., Monogr.* **5**, 184-197.

GRAHAM, U.M., BLUTH, G.J. & OHMOTO, H. (1988): Sulfide–sulfate chimneys on the East Pacific Rise, 11° and 13°N latitudes. 1. Mineralogy and paragenesis. *Can. Mineral.* **26**, 487-504.

HANNINGTON M.D. & GORTON, M.P. (1991): Analysis of sulfides for gold and associated trace metals by direct neutron activation with a low flux reactor. *Geostandards Newsletter* **15**, 145-154.

________, HERTZIG, P.M. & SCOTT, S.D. (1991): Auriferous hydrothermal precipitates on the modern seafloor. *In* Gold Metallogeny and Exploration (R.P. Foster, ed.). Blackie and Son Ltd., Glasgow, U.K. (249-282).

________ & SCOTT, S.D. (1988): Gold and silver potential of polymetallic sulfide deposits on the sea floor. *Marine Mining* **7**, 271-285.

________ & ________ (1989): Gold mineralization in volcanogenic massive sulfides: implications of data from active hydrothermal vents on the modern sea floor. *Econ. Geol., Monogr.* **6**, 491-507.

HARRIS, D.C., CABRI, L.J., & NOBILING, R. (1984): Silver-bearing chalcopyrite, a principal source of silver in the Izok Lake massive-sulfide deposit: confirmation by electron- and proton-microprobe analysis. *Can. Mineral.* **22**, 493-498.

HAYMON, R.M. (1983): Growth history of hydrothermal black smoker chimneys. *Nature* **301**, 695-698.

________ & KASTNER, M. (1981): Hot spring deposits on the East Pacific Rise at 21°N: preliminary description of mineralogy and genesis. *Earth Planet. Sci. Lett.* **53**, 363-381.

HEKINIAN, R., FEVRIER, M., BISCHOFF, J.L., PICOT, P. & SHANKS, W.C. (1980): Sulfide deposits from the East Pacific Rise near 21°N. *Science* **207**, 1433-1444.

________, FRANCHETEAU, J. & BALLARD, R.D. (1985): Morphology and evolution of hydrothermal deposits at the axis of the East Pacific Rise. *Oceanologica Acta* **8**, 147-155.

________, ________, RENARD, V., BALLARD, R.D., CHOUKROUNE, P., CHEMINÉE, J.L., ALBARÈDE, F., MINSTER, J.-F., CHARLOU, J.-L., MARTY, J.C. & BOULÈGUE, J. (1983): Intense hydrothermal activity at the rise axis of the East Pacific Rise near 13°N: submersible witnesses the growth of sulfide chimney. *Marine Geophys. Res.* **6**, 1-14.

________ & FOUQUET, Y. (1985): Volcanism and metallogenesis of axial and off-axial structures on the East Pacific Rise near 13°N. *Econ. Geol.* **80**, 221-249.

________, RENARD, V. & CHEMINÉE, J.L. (1984): Hydrothermal deposits on the East Pacific Rise near 13°N: geological setting and distribution of active sulfide chimneys. *In* Hydrothermal Processes at Seafloor Spreading Centers (P.A. Rona, K. Boström, L. Laubier, K.L. Smith, Jr., eds.). Plenum Press, New York, N.Y. (571-594).

JOHNSON, J.W., OELKERS, E.H. & HELGESON, H.C. (1992): SUPCRT92: a software package for calculating the standard molal thermodynamic properties of minerals, gases, aqueous species, and reactions from 1 to 5000 bar and 0 to 1000°C. *Comput. Geosci.* **18**, 899-947.

KNIGHTS, J.G. & PATTERSON, D.J. (1988): Process mineralogy of silver in lead–zinc–silver ores at Mount Isa, Australia. *In* Silver – Exploration, Mining & Treatment. Inst. Mining Metall., London, U.K. (101-110).

KOZLOV, V.K. (1985): Laboratory data on the role of carbonate complexes in hydrothermal silver transport. *Geochem. Int.* **22**(3), 85-95.

________ & KHODAKOVSKIY, I.L. (1983): The thermodynamic parameters of atomic silver in aqueous solutions at 25-280°C. *Geochem. Int.* **20**(3), 118-131.

________, KUZNETSOV, V.N, & KHODAKOVSKIY, I.L. (1983): The thermodynamic parameters of $Ag_2O_{(c)}$ and silver(I) hydroxy complexes in aqueous solution at elevated temperatures. *Geochem. Int.* **20**(1), 137-149.

LAROCQUE, A.C.L., JACKMAN, J.A., CABRI, L.J. & HODGSON, C.J. (1995): Calibration of the ion microprobe for the determination of silver in pyrite and chalcopyrite from the Mobrun VMS deposit, Rouyn–Noranda, Quebec. *Can. Mineral.* **33**, 361-372.

LEVIN, K.A. (1992): An experimental and thermodynamic study of the stabilities of silver chloride complexes in KCl and NaCl solutions up to 7 m at 300°C. *Geochem. Int.* **29**(5), 103-108.

MICHARD, G., ALBARÈDE, F., MICHARD, A., MINSTER, J.-F., CHARLOU, J.-L. & TAN, N. (1984): Chemistry of solutions from the 13°N East Pacific Rise hydrothermal site. *Earth Planet. Sci. Lett.* **67**, 297-307.

MOSS, R. & SCOTT, S.D. (1994): Distibution of silver in seafloor sulphide deposits of the East Pacific Rise. *Geol. Assoc. Can. – Mineral. Assoc. Can., Program Abstr.* **19**, A80.

ORTEGA-OSORIO, A. & PAEZ-OSUNA, F. (1989): Composición geoquímica y mineralógica de los depósitos hidrotermales de la dorsal del Pacífico Mexicano (21N) y la Cuenca de Guaymas. *Geofisica Internacional* **28**, 737-762.

OUDIN, E. (1987): Trace elements and precious metal concentrations in East Pacific Rise, Cyprus and Red Sea submarine sulfide deposits. *In* Marine Minerals (P.G. Teleki, M.R. Dobson, J.R. Moore, & U. Von Stackelberg, eds.). *NATO Adv. Study Inst., Ser. C* **194**, 349-362. D. Reidel Publ. Co., Dordrecht, The Netherlands.

PERKINS, E.H., KHARAKA, Y.K., GUNTER, W.D. & DEBRAAL, J.D. (1989): Geochemical modeling of water–rock interactions using SOLMINEQ.88. *In* Chemical Modeling of Aqueous Systems II (D.C. Melchior & R.L. Bassett, eds.). *Am. Chem. Soc., Symp. Ser.* **416**, 117-127.

RONA P.A. & SCOTT, S.D. (1993): A special issue on sea-floor hydrothermal mineralization: new perspectives, Preface. *Econ. Geol.* **88**, 1935-1975.

RUAYA, J.R. & SEWARD, T.M. (1986): The stability of chlorozinc(II) complexes in hydrothermal solutions up to 350°C. *Geochim. Cosmochim. Acta* **50**, 651-661.

SCOTT, S.D. (1983): Chemical behaviour of sphalerite and arsenopyrite in hydrothermal and metamorphic environments. *Mineral. Mag.* **47**, 427-435.

________ & BARNES, H.L. (1971): Sphalerite geothermometry and geobarometry. *Econ. Geol.* **66**, 653-669.

SEWARD, T.M. (1976): The stability of chloride complexes of silver in hydrothermal solutions up to 350° C. *Geochim. Cosmochim. Acta* **40**, 1329-1341.

________ (1984): The formation of lead (II) chloride complexes to 300°C: a spectrophotometric study. *Geochim. Cosmochim. Acta* **48**, 121-134.

SHARP, T.G. & BUSECK, P.R. (1993): The distribution of Ag and Sb in galena: inclusions versus solid solution. *Am. Mineral.* **78**, 85-95.

SPIESS, F.N., MACDONALD, K.C., ATWATER, T., BALLARD, R., CARRANZA, A., CORDORBA, D., COX, C., DIAZ GARCIA, V.M., FRANCHETEAU, J., GUERRERO, J., HAWKINS, J., HAYMON, R., HESSLER, R., JUTEAU, T., KASTNER, M., LARSON, R., LUYENDYK, B., MACDOUGALL, J.D., MILLER, S., NORMARK, W., ORCUTT, J. & RANGIN, C. (1980): East Pacific Rise: hot springs and geophysical experiments. *Science* **207**, 1421-1432.

SUGAKI, A., SCOTT, S.D., HAYASHI, K. & KITAKAZE, A. (1987): Ag_2S solubility in sulfide solutions up to 250°C. *Geochem. J.* **21**, 291-305.

TIVEY, M.K. & MCDUFF, R.E. (1990): Mineral precipitation in the walls of black smoker chimneys: a quantitative model of transport and chemical reaction. *J. Geophys. Res.* **95**, 12,617-12,637.

TURNER, J.S. & CAMPBELL, I.H. (1987): A laboratory and theoretical study of the growth of "black smoker" chimneys. *Earth Planet. Sci. Lett.* **82**, 36-48.

VON DAMM, K.L. (1983): *Chemistry of Submarine Hydrothermal Solutions at 21° North, East Pacific Rise and Guaymas Basin, Gulf of California.* Ph.D. thesis, Massachusetts Inst. Technology – Woods Hole Oceanographic Inst., Woods Hole, Massachusetts, **WHOI-84-3**.

________ (1988): Systematics of and postulated controls on submarine hydrothermal solution chemistry. *J. Geophys. Res.* **93**, 4551-4561.

________ (1990): Seafloor hydrothermal activity: black smoker chemistry and chimneys. *Annu. Rev. Earth Planet. Sci.* **18**, 173-204.

________, EDMOND, J.M., GRANT, B., MEASURES, C.I., WALDEN, B. & WEISS, R.F. (1985a): Chemistry of submarine hydrothermal solutions at 21°N, East Pacific Rise. *Geochim. Cosmochim. Acta* **49**, 2197-2220.

________, ________, MEASURES, C.I. & GRANT, B. (1985b): Chemistry of submarine hydrothermal solutions at Guaymas Basin, Gulf of California. *Geochim. Cosmochim. Acta* **49**, 2221-2237.

ZIERENBERG, R.A. & SCHIFFMAN, P. (1990): Microbial control of silver mineralization at a sea-floor hydrothermal site on the northern Gorda Ridge. *Nature* **348**, 155-157.

________, SHANKS, W.C. & BISCHOFF, J.L. (1984): Massive sulfide deposits at 21° N, East Pacific Rise: chemical composition, stable isotopes and phase equilibria. *Geol. Soc. Am., Bull.* **95**, 922-929.

ZOTOV, A.V., LEVIN, K.A., KHODAKOVSKIY, I.L. & KOZLOV, V.K. (1986a): Thermodynamic parameters of Ag(I) chloride complexes in aqueous solution at 273–623K: *Geochem. Int.* **23**(9), 103-116.

________, ________, ________ & ________ (1986b): Thermodynamic parameters of Ag^+ in aqueous solution at 273–573°K. *Geochem. Int.* **23**(3), 23-33.

________, ________, KOTOVA, Z.Y. & VOLCHENKOVA, V.A. (1982): An experimental study of silver hydroxychloride complexes in hydrothermal solutions. *Geochem. Int.* **19**(4), 151-164.

Received April 20, 1995, revised manuscript accepted April 10, 1996.